Angewandte Chemie
Eine Zeitschrift der Gesellschaft Deutscher Chemiker

Supporting Information

Exploring the Druggability of Conserved RNA Regulatory Elements in the SARS-CoV-2 Genome

*Sridhar Sreeramulu[+], Christian Richter[+], Hannes Berg, Maria A. Wirtz Martin, Betül Ceylan, Tobias Matzel, Jennifer Adam, Nadide Altincekic, Kamal Azzaoui, Jasleen Kaur Bains, Marcel J. J. Blommers, Jan Ferner, Boris Fürtig, Michael Göbel, J. Tassilo Grün, Martin Hengesbach, Katharina F. Hohmann, Daniel Hymon, Bozana Knezic, Jason N. Martins, Klara R. Mertinkus, Anna Niesteruk, Stephen A. Peter, Dennis J. Pyper, Nusrat S. Qureshi, Ute Scheffer, Andreas Schlundt, Robbin Schnieders, Elke Stirnal, Alexey Sudakov, Alix Tröster, Jennifer Vögele, Anna Wacker, Julia E. Weigand, Julia Wirmer-Bartoschek, Jens Wöhnert, and Harald Schwalbe**

anie_202103693_sm_miscellaneous_information.pdf
anie_202103693_sm_xlsx_Dateien.zip

Suppl. Information

Material and Methods

RNA synthesis for NMR experiments: Fast parallelized RNA production was established for the SCoV-2 project as described.[1] In brief, RNA coding sequences were cloned into a HDV-containing vector and RNAs were prepared by T7 *in-vitro* transcription from amplified and linearized plasmid templates. Following RNA purification by polyacrylamide (PAA) gel electrophoresis, residual PAA was removed by high-pressure liquid chromatography (HPLC) to avoid non-specific interactions between fragments and PAA in the screening experiments. RNA purity and homogeneity of above 95% was validated by denaturing and native PAA gel electrophoresis, respectively.

Screening sample preparation: The DSI-poised fragment library contains 768 compounds of which 106 contain ^{19}F atoms.[2] The high chemical diversity of the DSI-poised library allowed us to prepare mixtures containing 12 randomly chosen fragments without any significant chemical shift overlap in the ^{1}H-observed NMR spectra (Suppl. Figure S1). Each fragment mixture contained 12 fragments at a nominal concentration of 4.2 mM each in 90% d_6-DMSO with 10% D_2O. In total, the 768 fragments accounted for 64 mixtures. 190 µl of a 10 µM RNA in screening buffer (25 mM KPi, 50 mM KCl, pH 6.2) was manually pipetted into 3 mm NMR tubes. 10 µl of the fragment mixture was added using a pipetting robot to a final concentration of 200 µM for each fragment. As a result of the mixture added, the final d_6-DMSO concentration was 5%, which served as the NMR lock solvent. The total sample volume was 200 µl, with an [RNA]:[ligand^{each}]-ratio of 1:20. For 659 fragments, the nominal concentration of 4.2 mM could be reached in screening buffer, while the other fragments were less soluble in this buffer that was optimized for RNA screening. Approximately 50 fragments showed additional signals suggesting partial chemical degradation of the fragment.

NMR spectroscopy: For the measurements, 5% DMSO was used for locking the NMR spectrometer frequency. Shim optimization was performed on the H_2O signal by using a home-built script for ^{1}H gradient shimming. In screening experiments, the residual water signal was suppressed using the SOGGY sequence, which was implemented in all screening pulse sequences (Suppl. Table S2, Suppl. Figure S2). From our experience, application of the composite water pulse makes this method more robust than conventional excitation sculpting in case of air bubbles in the NMR tube or tubes with smaller filling height. All screening experiments were performed by using 3 mm tubes in a 5 mm cryogenic probe.
Two mixing times (5 ms, 100 ms) with a bandwidth of the CPMG-pulse of 6.25 kHz were recorded for ^{1}H-R_2-CPMG experiments. Mixing times of 0, 200 and 400 ms CPMG with a bandwidth of 68 kHz using an adiabatic shape were used for ^{19}F-R_2-CPMG experiments. R_2-CPMG pulse sequences were performed using temperature compensation. All these experiments detected changes of ligand signals in the presence of substoichiometric RNA target.

Quantification of fragment hits:

Quantification of chemical shifts: Chemical shift perturbation in Hertz [Hz] was measured as chemical shift difference induced by addition of 1/20th RNA target. Quantitative analysis of waterLOGSY and T_2 was performed as described previously.[3,4] One well resolved proton signal corresponding to each of the fragment was chosen for analysis.

Quantitative analysis of the waterLOGSY: The LOGSY-factor was derived from the equation below, wherein the difference between the absolute peak intensity of the ligand in the presence of target (I_{Target}) and absence ($I_{Reference}$) was divided by the peak intensity of the reference ($I_{Reference}$). If the

intensities are equal or ($I_{Reference}$) has no intensity will lead to null LOGSY effect or 1, respectively and is defined as no binding.

$$LOGSY\ factor = \ ABS\ \frac{\left(I_{Target} - \left(I_{Reference}\right)\right)}{I_{Reference}}$$

Quantitative analysis of T_2: The T_2-reduction is the partial loss of ratios from relative peak integrals between 100 ms CPMG and 5 ms CPMG of a proton signal in the ^{1}H spectra of the fragment in the presence and absence of the RNA given as percentage and is calculated as below. If the T_2-reduction of a fragment in the presence of RNA is ≥ 20%, then it is considered as a binder.

$$T_2 - reduction\ (\%) = \left[1 - \frac{\frac{Peak\ integral\ Target^{100ms}}{Peak\ integral\ Reference^{100ms}}}{\frac{Peak\ integral\ Target^{5ms}}{Peak\ integral\ Reference^{5ms}}}\right] \times 100$$

NMR-titrations: For each titration step a separate 40 µL NMR sample was prepared. Each Sample contained 100 µM Ligand varying the RNA concentration from 0 - 250 µM in the screening buffer (25 mM KPi, 50 mM KCl, pH 6.2) with 5 % DMSO-d6. While keeping the ligand concentration constant, the following RNA concentrations were used as titration steps: 0, 10, 20, 35, 50, 100 and 250 µM. 100 µM DSS was used as internal reference. Stock solutions used to prepare the samples contained 1 mM Ligand in screening buffer and 5 % DMSO-d6 or 300 – 400 µM RNA in screening buffer respectively. All NMR measurements were carried out in 1.7 mm NMR-tubes and at 293 K. The changes in CSPs were analyzed using non-linear fitting and chose one site specific binding equation to derive the dissociation constant (K_D).

NMR-binding site mapping: ^{1}H-^{15}N-BEST-TROSY spectra was obtained with a 50 µM ^{15}N-labeled pseudoknot. The spectra were acquired at 298 K and recorded on a Bruker AV 800 MHz (Buffer: 25 mM KPi, pH 6.2, 50 mM KCl, 5% D2O). Ligand D01 was added stepwise in molar ratios from 0.5 to 4 equivalents in 5 steps (final d6-DMSO concentration 1%). Control experiments were performed for each titration point (0 eq D01, 0% d6 DMSO till 4 eq D01, 1% d6-DMSO). ^{1}H-^{13}C-HSQC spectra were obtained with a 200 µM ^{13}C^{15}N – (A, U) selectively labeled pseudoknot. The spectra were acquired at 298 K on a Bruker AV3 HD 600 MHz (Buffer: 25 mM KPi, pH 6.2, 50 mM KCl, 3% (v/v) d6-DMSO). Ligand D01 was added stepwise in molar ratios from 0.5 to 4 equivalents in 4 steps (Final d6-DMSO concentration 13%). Reference spectra (0 eq D01, 13% d6-DMSO) and end point (4 eq D01, 13% d6-DMSO) were overlayed.

Fluorescence measurements: All fluorescence measurements were performed on a Tecan Spark® multimode microplate reader. D01 emission fluorescence was monitored at a wavelength of 440 nm after exciting at 360 nm. For the titrations, D01 concentration (0.5 µM) were kept constant, while the RNA concentration was varied from 0 to 200 molar equivalents in 11 steps. The decrease in fluorescence at 440 nm was monitored. The normalized percent fluorescent changes were analyzed using non-linear fitting and chose one site specific binding equation to derive the dissociation constant (K_D).

In-line probing

SARS-CoV-2 Pseudoknot RNA (69mer) + Cy5-T10-R8 + DNA Splint

5′Cy5-TTTTTTTTTTGGCCAGUA●GGCGGUGUAAGUGCAGCCCGUCUUACACCGUGCGGCACAGGCACUAGUACUGAUGUCGUAUACAGGGCU

3′ CCGGTCAT●CCGCCACATTCA

The detailed procedure is described elsewhere [5]. In brief:

Labeling of SARS-CoV-2 pseudoknot RNA

Annealing of oligonucleotides. The oligonucleotide mixture of GMP-primed SARS-CoV2 Pseudoknot RNA (30 pmol/µL), Cy5-labeled DNA/RNA chimera (30 pmol/µL) and DNA splint (45 pmol/µL) in 50 mM Tris-HCl buffer (pH 7.5) containing 2 mM $MgCl_2$, 1 mM DTT and 400 µM ATP was annealed in a thermocycler. After an initial denaturation step at 90 °C for 5 min the samples were cooled down to 30 °C with a rate of 0.1 °C/s.

Ligation [6]. Each aliquot of the annealed oligonucleotide mixture was diluted with 50 mM Tris-HCl buffer (pH 7.5) containing 2 mM $MgCl_2$, 1 mM DTT and 400 µM ATP to an RNA concentration of 10 pmol/µL. After addition of 0.1 nmol T4 RNA Ligase 2 per nmol of RNA [7] the ligation mixture was incubated at 37 °C for 2 h. The ligation product (Cy5-T10-R8- SARS-CoV-2 Pseudoknot RNA,) was purified by 8% denaturing PAGE.

In-line probing [8]

In-line probing was carried out in presence or absence of ligands. Because the ligands are insoluble in water or aqueous buffers DMSO was applied as a solving assistant (final DMSO concentration 20%). In a total volume of 8 µL Cy5-T10-R8- SARS-CoV2 pseudoknot RNA (final concentration 150 nM) was pre-incubated at 37°C for 10 min together with the ligand (final concentration 100 µM). Controls contained 20% DMSO instead of ligand. After that in-line probing buffer (50 mM Tris-HCl (pH 8.3), 20 mM MgCl2, 100 mM KCl) was added and the samples were incubated for 24 h at 37 °C. In an additional set of control reactions, the in-line probing buffer was replaced by 50 mM Tris-HCl (pH 8.0) buffer. The fragmentation pattern was analyzed on a DNA sequencing device (ALFexpress, Amersham Biosciences) and the outcome was compared with a hydrolysis ladder of Cy5-labeled T10-R8-SARS-CoV2 Pseudoknot RNA.

Suppl. Table 1: **Analysis of loops and bulges in the SCoV-2-genome**[9,10]

RNA element	Loop sequences (nt numbers)	# in genome[9] / # predicted in structured regions[10]	# single stranded in structured regions / # as apical loop <10 nts / experimental[1]	SCoV-2 conservation loop sequences[11]
5_SL1	UCCC$_{18\text{-}21}$	29 / 16	4 / 1	100%
5_SL2	CUUGU$_{50\text{-}54}$	67 / 43	3 / 3	100%
5_SL3	UCUAAAC$_{65\text{-}71}$	5 / 2	1 / 1	100%
5_SL4	UGCAU$_{104\text{-}108}$	29 / 15	2 / 1	100%
5_SL5a	UUUC**G**U$_{200\text{-}205}$	3 / 3	3 / 2	2% G**204**T
5_SL5b	UUU**C**GU$_{238\text{-}243}$	3 / 3	3 / 2	99% C**241**T
5_SL5c	GAAA$_{256\text{-}259}$	166 / 97	<6 nts: 35 / 16	100%
5_SL6	UUUUA$_{324\text{-}328}$	90 / 45	14 / 2	100%
5_SL7	GUGGA$_{368\text{-}373}$	26 / 19	2 / 1	100%
5_SL8	GU**U**UU$_{443\text{-}447}$	79 / 38	5 / 1	12% T**445**C
attHP	UCAG$_{13.442\text{-}13.445}$	116 / 58	11 / 3	100%
PK	GCACUAGUA$_{13.524\text{-}13.522}$	1 / 1	0 / 0 / **1**	100%
3_SL1	CUUUUC$_{29.580\text{-}29.585}$	15 / 9	5 / 3	100%
3_SL2	AGCACAA**G**UAG$_{29.638\text{-}29.648}$	1 / 1	0 / 0 / **1**	11% G**29645**T
3_SL3base	n.a.	1 / 0	0 / 0 / **1**	
3_s2m	GA**G**UAC**G**AU$_{29.745\text{-}29.753}$	2 / 1	0 / 0 / **1**	4% G**29751**T 1% G**29747**T

RNA element	Bulge sequences >4 nts (nt numbers)	# in genome[9] / # predicted in structured regions[10]	# as single stranded sequence <8nt / predicted vs. experimental[1]	SCoV-2 conservation bulge sequences[11]
5_SL1 to 5_SL5b+c	n.a			
5_SL5stem	n.a			3% G**174**T
5_SL6	CAACU**C**AGUUU$_{308\text{-}318}$	9 / 5 [CAACUCA]	0 / **1**	2% C**313**T, 3% C**335**T
5_SL7	n.a			
5_SL8	(A)AAAA$_{(434)435\text{-}339}$	203 / 103 x A_4; 60 / 34 x A_5	23x A_4, 12x A_5	100%
attHP	n.a			
PK	AUACA$_{13.533\text{-}13.537}$	47 / 25	6	100%
3_SL1	G**C**AGA$_{29.554\text{-}29.558}$	38 / 27	1	1% C**29555**T
3_SL2	n.a			
3_SL3base	UAGCUUCUUAG$_{29.851\text{-}29.861}$	1 / 0	0 / **1**	100%
3_s2m	C**G**AGGC$_{29.733\text{-}29.738}$	1 / 0	0 / **1**	2% G**29734**C

Suppl. Figure S1: Secondary structures that define RNA target structure space. The experimentally derived secondary structures of all screened RNA elements (5_SL1 to 3_s2m, construct names as described previously[1]) are shown. A-helical structures are boxed. Other structural motifs are illustrated as follows: I) blue: capping loops; II) green: asymmetric internal loops and bulges; III) grey: highly structured capping loops; IV) orange: non-canonical base-pairs or mismatches (may or may not disturb A-helix conformation); V) pink: single-stranded three-helix junctions.

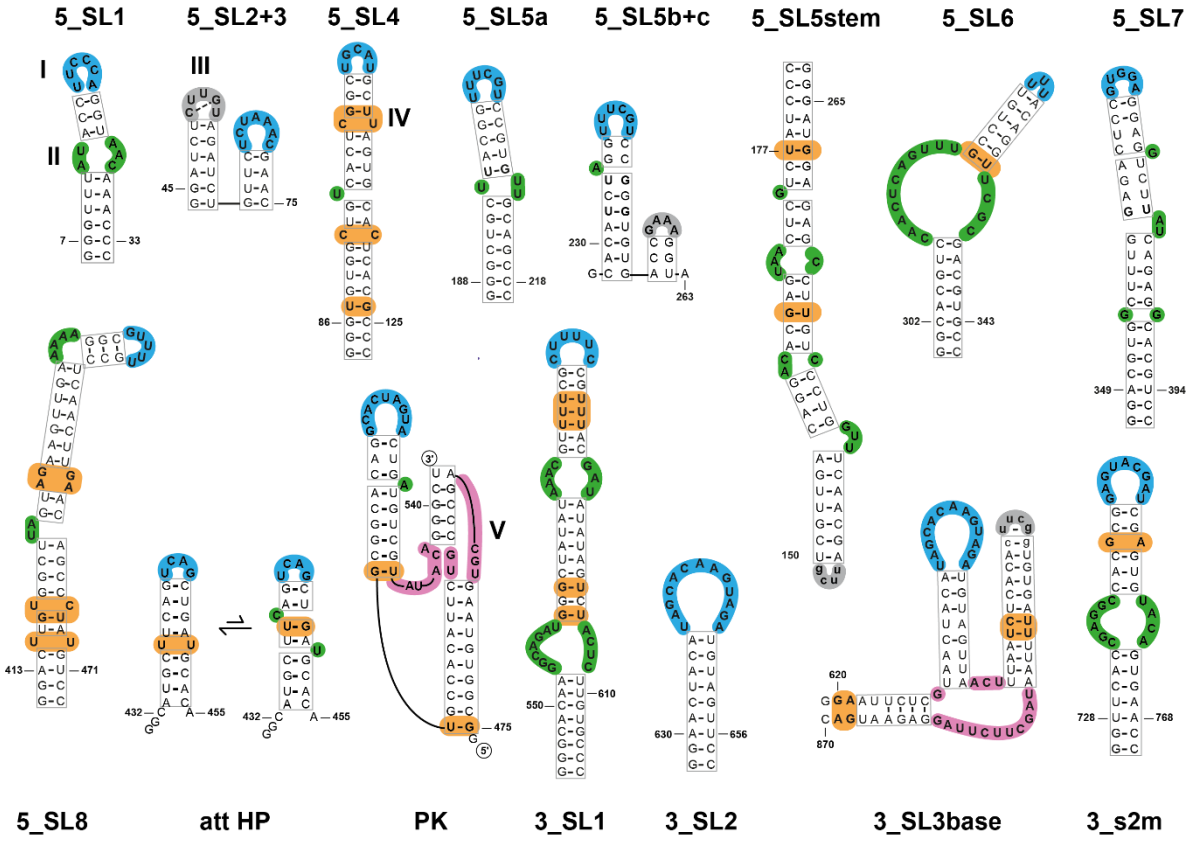

Suppl. Table 3: A,U,G,C content in representative sequences stretches of SCoV-2.

motif analysis	genome[9]	loops (n=15)	bulges (n=6)
average size (nts)	29.903	5,9	7,2
nt composition (%)			
U	**32**	**38**	**24**
C	18	19	21
G	20	19	19
A	**30**	**24**	**36**

Suppl. Figure S2: NMR spectra of a representative mixture of 12 ligands from the 768 fragment containing DSI library: ^{1}H-NMR spectrum of an exemplary mixture (A3-Mix): A and B display an overlay of the ^{1}H-NMR spectrum of the single compounds (black) and the A3-mix (blue) of the aliphatic and aromatic regions, respectively. In C, the chemical structure of the individual compounds in the A3-mix are shown. 1D spectra were acquired with water suppression at 600 MHz. The temperature was set to 298 K for the single compound and 293 K for the mixture. In the figure, signals marked with * result from contamination or from additional solvent. Signals marked with # result from different protonation states of ligand A08.

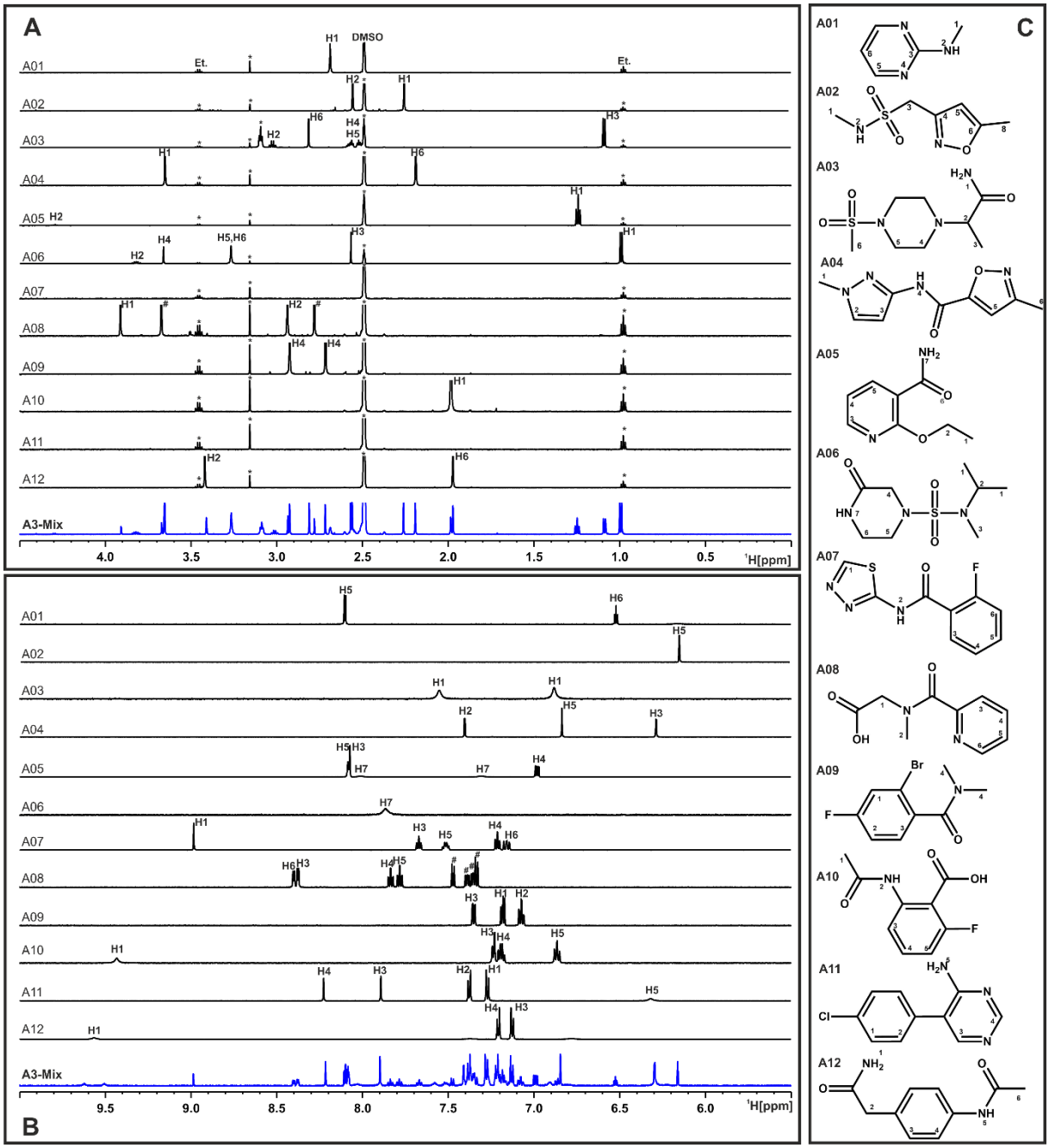

Suppl. Figure S3: Optimization of NMR sequences and parameters for ligand-based NMR screening

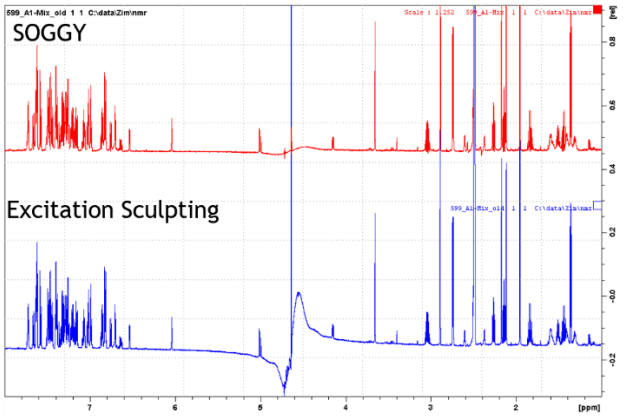

Optimization of water suppression: Representative 1D spectra of the fragment mix using the SOGGY (red) and ES (blue) sequence for the water suppression. The experiments were recorded at 600 MHz with 128 scans.

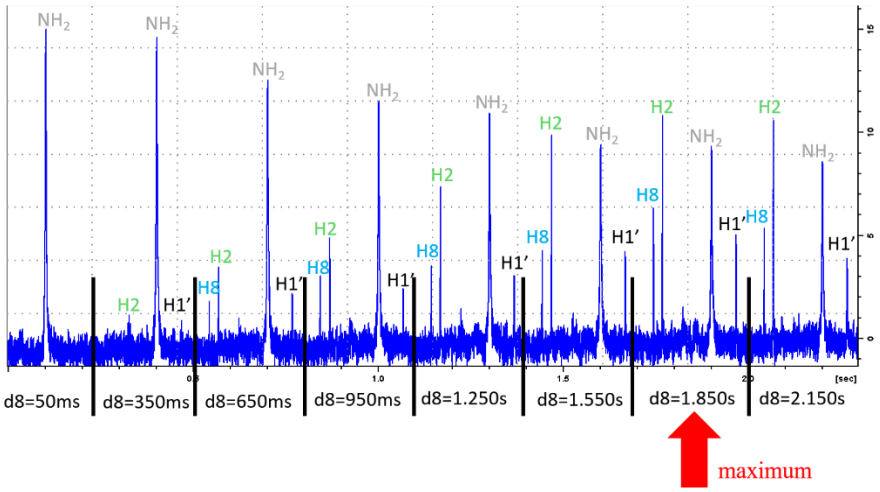

Optimization of waterLOGSY mixing time: Optimizing mixing time in the waterLOGSY experiment. The optimization was done for a complex sample containing 1 mM AMP-PNP + 10 uM EPHA2 Kinase (34 kDa). The experiments were recorded at 600 MHz using 128 scans.

Suppl. Table 4: NMR experiments to screen the RNA. Each sample for the ^{1}H-sreening was measured for 45 min

#	NMR experiments*	Sample utilized Solvents	Experiment-specific parameter settings	MT
1	^{1}H 1D	^{1}H 1D with water suppression SOGGY[12,13]	Excitation sculpting with a composite 180° spin echo pulse. The SOGGY pulse was implemented. NS = 64.	4.5 min
2	water-LOGSY on ^{1}H	waterLOGSY with SOGGY sequence for water suppression[14,15]	The SOGGY sequence was implemented in the standard waterLOGSY sequence. The mixing time was set to 1.85 ms NS = 320.	27 min
3, 4	T_2 CPMG on ^{1}H	T_2 relaxation using a pseudo2D sequence with CPMG spinlock field of 6.25kHz (5 and 100 ms) with temperature compensation.	The SOGGY sequence was implemented in the standard CPMG sequence. NS = 128.	13 min.

MT, measurement time. NS, number of scans. During the screen, sample mixes were stored at 4 °C. The experiments were conducted at 600 MHz and 293K in RNA buffer (25 mM KPi, 50 mM KCl, pH 6.2) in 94.5% H_2O / 4.5% d_6-DMSO in a 3 mm tube. *pulse sequence and parameter set for in-house optimized experiments can be obtained upon request and data sets can be downloaded at covid19-nmr.de.

Suppl. Figure S4: Quantification of chemical shift perturbation (CSP), LOGSY factor and T_2-reduction upon addition of 20-fold access of ligand over RNA at an RNA concentration of 10 μM.

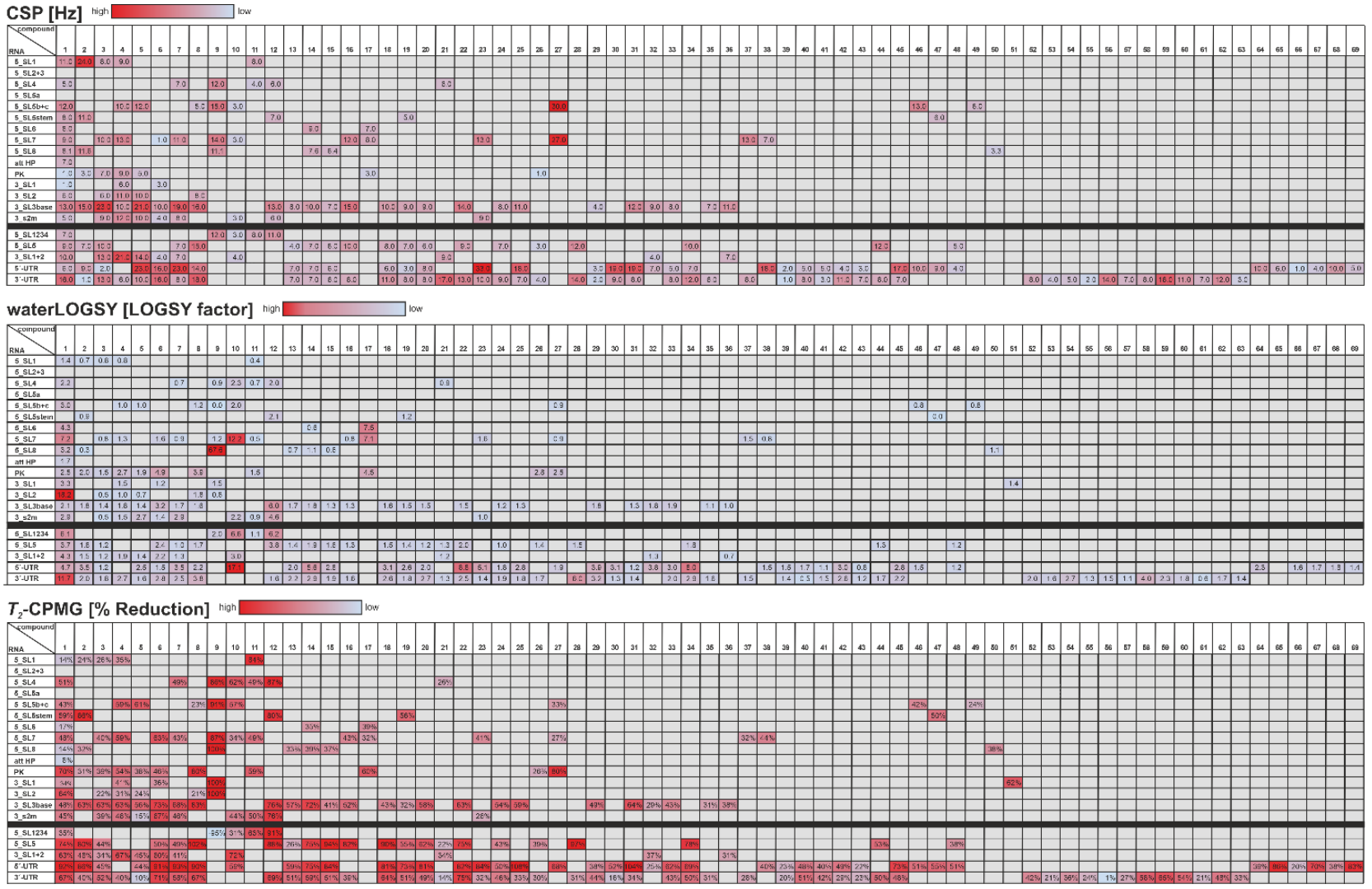

Suppl. Table 5: Analysis of privileged RNA target space.

RNA	structure space (2S) score (in bits)[16]	Hit Frequency (HF)	druggability score (2S x HF)	expected therapeutic relevance
5_SL1	22	5	110	++
5_SL2+3	24	0	0	++
5_SL4	20	7	140	++
5_SL5a	18	0	0	+
5_SL5b+c	22	9	198	+
5_SL5stem	20	5	100	o
5_SL6	36	3	108	o
5_SL7	20	14	280	o
5_SL8	38	7	266	o
att HP	12	1	12	++
PK	40	11	440	++
3_SL1	48	4	192	+
3_SL2	26	6	156	+
3_SL3base	64	25	1600	++
3_s2m	42	10	420	+

Analysis of privileged RNA target space: According to [16], non-helical regions of the RNAs were evaluated by addition of individual position uncertainties, which is 1.93 bits for loop nucleotides and 1.95 for bulge nucleotides. For the sake of clarity, we simplified the structure space score to 2 bits per single-stranded nucleotide position. The druggability score results from the weighting of unique single-stranded sequence space (=structure space) with the experimentally found number of hits.

Suppl. Table 6: Molecular descriptors distinguishing between hits and non-hits.

Descriptors	Calculated LogP		Polar Surface Area		Molecular Weight		Number of HBD		Number of HBA		Number of Amide Bonds		Number of Atoms		Number of Aromatic Rings		Fraction_SP3	
	non-hits	Hits	non-hits	Hits	non-hits	Hits	non-hits	Hits	non-hits	Hits	non-hits	Hits	non-hits	Hits	non-hits	Hits	non-hits	Hits
number of compounds	699	69	699	69	699	69	699	69	699	69	699	69	699	69	699	69	699	69
Mean	1.48	2.03	48.16	51.36	208.00	214.03	1.06	1.26	2.86	3.10	0.71	0.59	28.36	27.33	1.12	1.90	0.44	0.20
Std. Deviation	1.03	0.85	18.03	14.35	33.23	26.85	0.69	0.68	1.07	0.89	0.70	0.63	5.02	3.65	0.65	0.62	0.26	0.17
Minimum	-1.56	0.28	3.24	12.03	109.06	139.08	0	0	1	1	0	0	14	19	0	1	0	0
Maximum	3.61	3.49	128.36	90.89	334.08	249.06	4	3	6	5	4	2	42	36	3	3	1	0.64

Suppl. Figure S5: Chemical structure of 29 fragments that bind to the larger RNA elements: 5'-UTR and 3'-UTR.

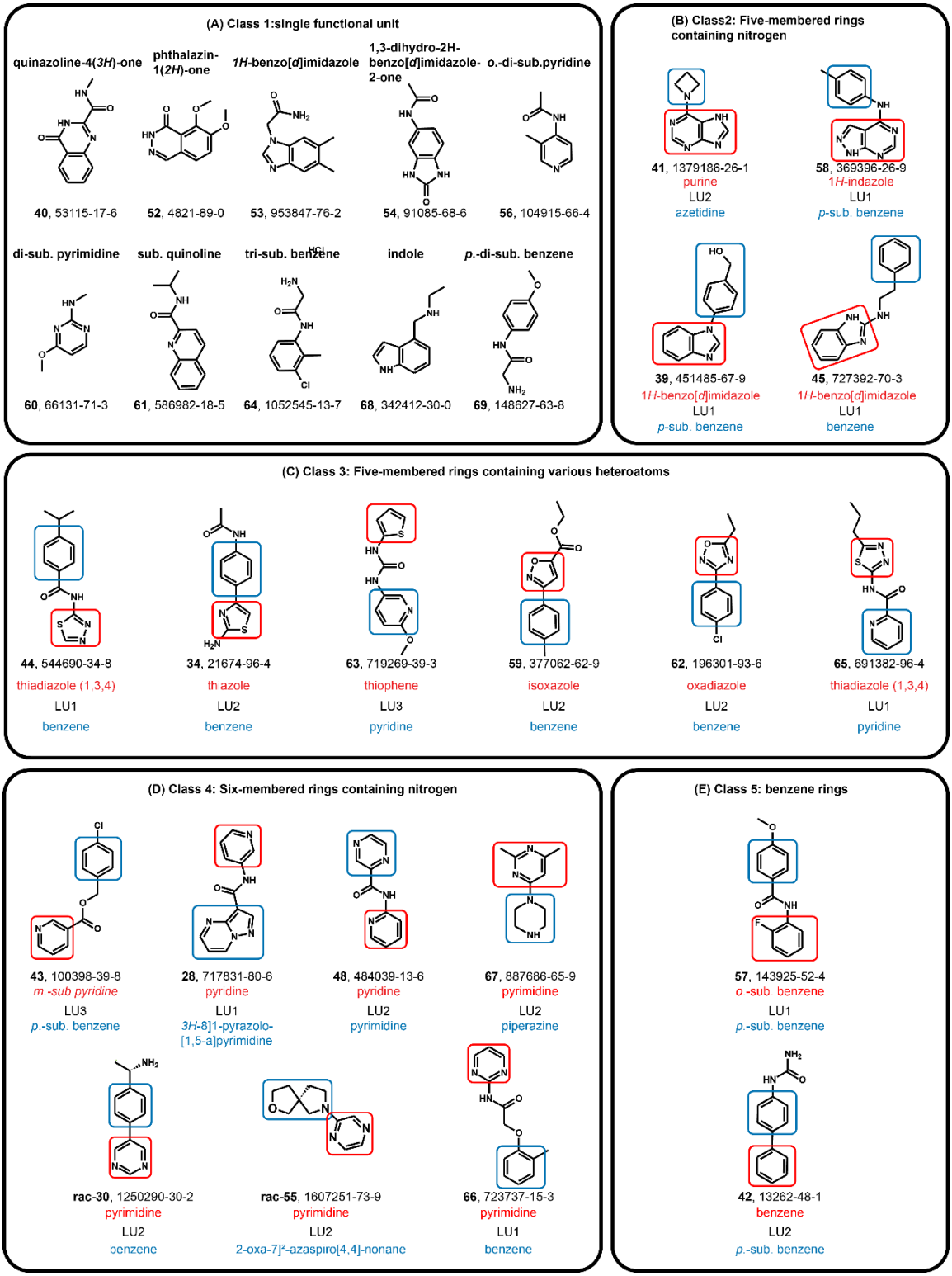

Suppl. Figure S6: Matrix dissecting functional units found for 40 hits targeting 15 RNA elements of SCoV-2. On the diagonal, we identify the number of occurrences of an individual functional unit among the 40 hits binding to the 15 RNA targets. Below the diagonal, the number of hits bearing the combination of the two functional units along with their identities in parentheses is indicated and is given for the 30 compounds. Above the diagonal, the corresponding RNA elements, to which the hit binds, are given. Coloring of the cells across the diagonal is consistent to identify hits and their corresponding target RNA elements.

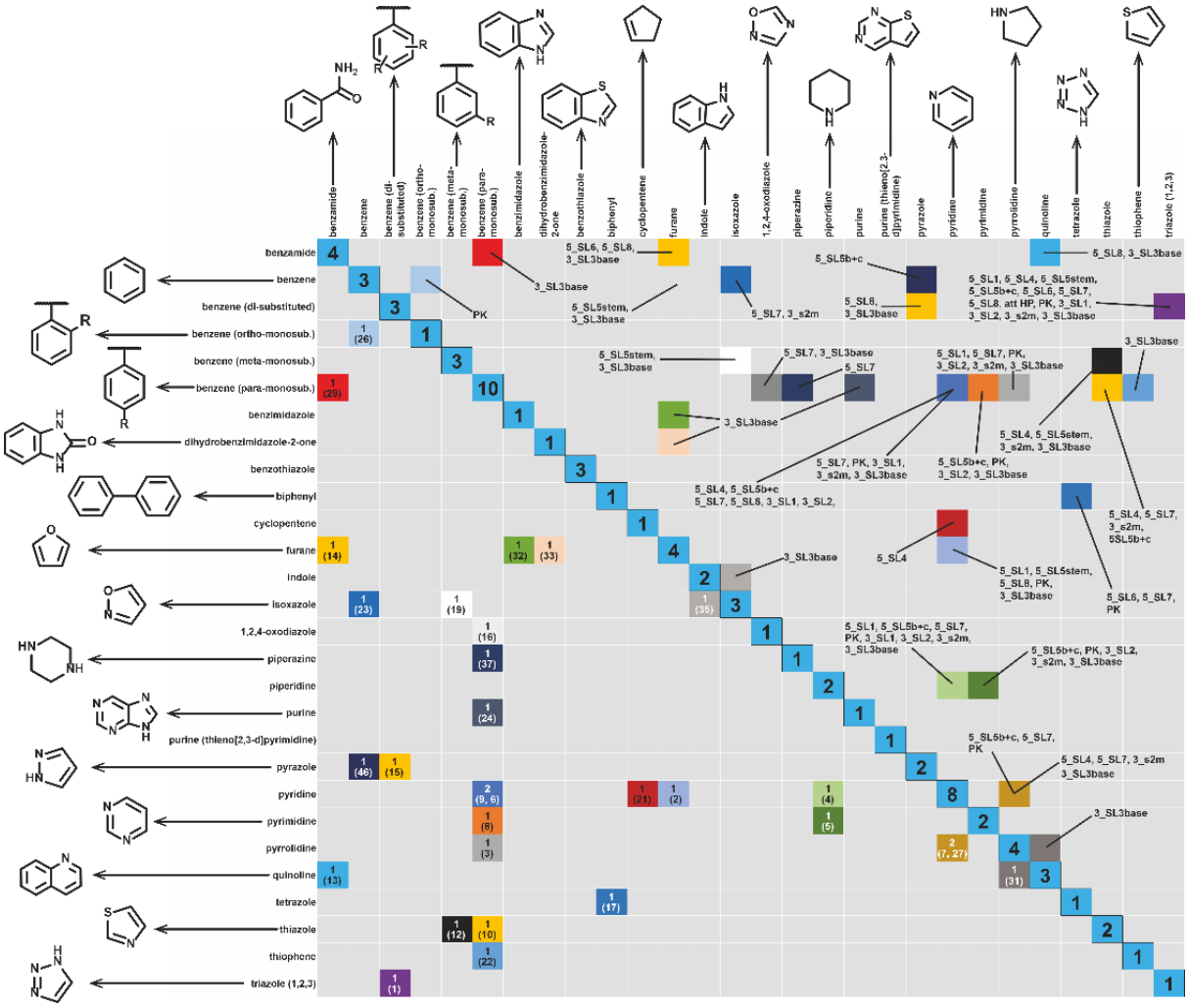

Suppl. Figure S7: NMR and fluorescence-based determination of dissociation constants for fragment hits and follow-up compounds. NMR-based (Ligand-observed; protons chosen to follow CSP are indicated) titration curves for the interaction of binders with 3_s2m (compounds 1, 3, 4, 5, 6, 10, 11 and 23) and PK (compounds 2, 3, 4, and 5) and. The fluorescence-based titration curves were used for determining the dissociation constants of D01 with PK and 3_s2m.

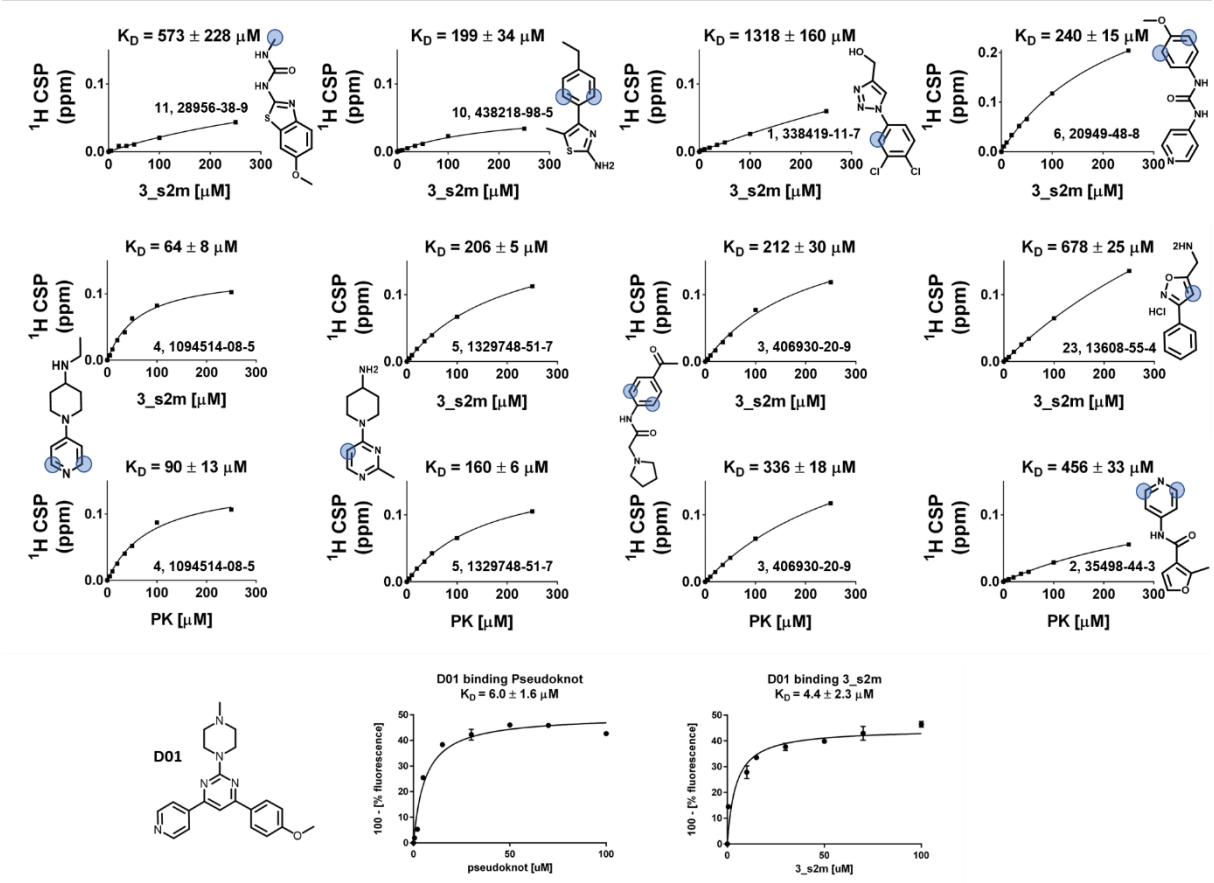

Suppl. Figure S8: Control experiments to access D01 specificity. Fluorescence-based titration curves were used for examining D01 interacting with various control RNA sequences (Poly-A, Poly-U, structured 14mer RNA stem-loop [“UUCG”], and scrambled RNA [ligation oligo used for inline probing; sequence: 5’-GGCCAGUA-3’). No saturable binding was observed, suggesting that D01 does not bind to any of the control RNAs. The average fluorescence across the varying concentrations of RNA is shown with a running dashed line.

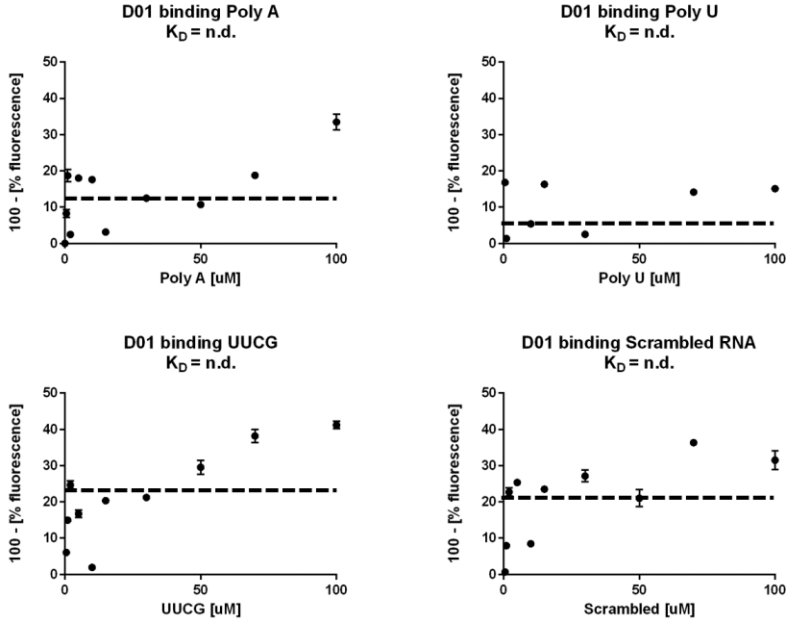

Suppl. Figure S9: 2D NMR-observed interaction of binder fragment 8 (133256-51-6) and 2D NMR- and in-line probing-observed interaction of D01 to the PK of SCoV-2. A, ^{1}H, ^{13}C-HSQC of PK apo (black) and in the presence of 4 equivalents of fragment 8 (133256-51-6) (green). Fragment 8 binds with a K_D of 46 µM (A, inset titration curve). B, ^{1}H, ^{13}C-HSQC of PK apo (black) and in the presence of 4 equivalents of D01 (green). Additionally, 1D traces of the signals showing changes (CSP or line broadening) are displayed as insets. Addition of D01 to PK results in CSPs or line broadening beyond detection. C, Inline-probing profile of D01-treated PK (light green) vs. DMSO-only treated PK (dark green, both upper trace), PK-alkaline digestion ladder (middle trace) and PK-untreated control (lower trace). Changes of cleavage pattern are mapped as green nucleotides on the 2D structure (left).

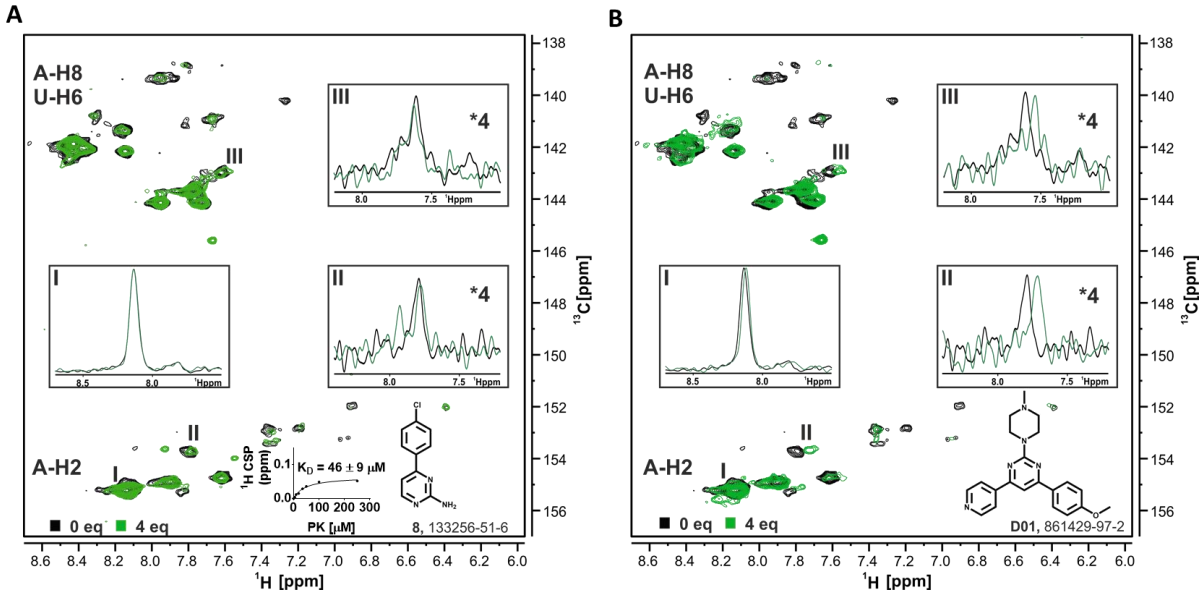

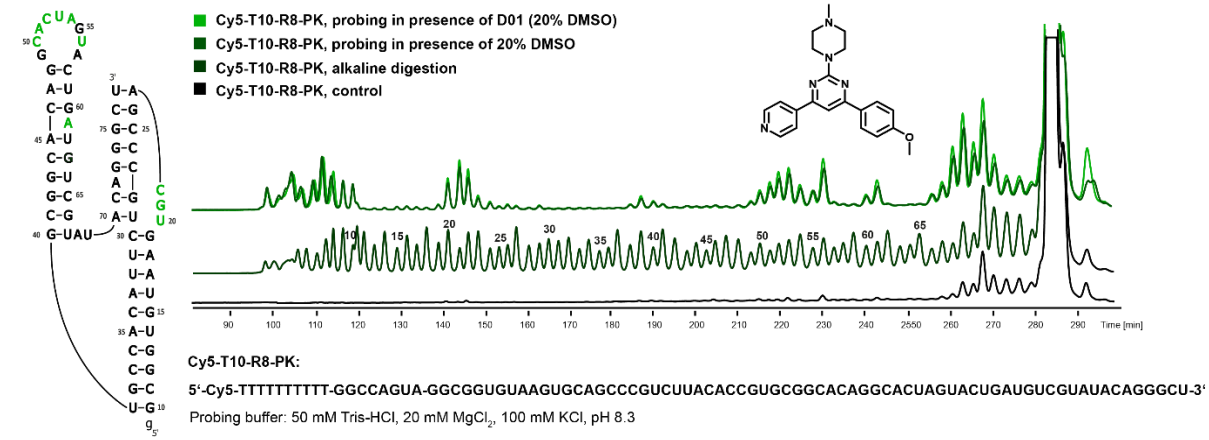

Suppl. Table 7: Distribution of the functional units across the library for hits and non-hits.

Functional units present in	Hits	Non-hits	Sum	% in hits	% in non-hits
Benzene (di-substituted-ortho)	3	51	54	5.6%	94.4%
Benzene	59	408	467	12.6%	87.4%
Benzamide	8	52	60	13.3%	86.7%
Benzene (para-monosub.)	28	1784	1812	1.5%	98.5%
Benzene (meta-monosub.)	7	109	116	6.0%	94.0%
Benzene (ortho-monosub.)	11	131	142	7.7%	92.3%
Benzimidazole	6	16	22	27.3%	72.7%
Furan	4	24	28	14.3%	85.7%
Isoxazole	4	26	30	13.3%	86.7%
Piperazine	2	49	51	3.9%	96.1%
Piperidine	2	72	74	2.7%	97.3%
Pyrazoline	4	49	53	7.5%	92.5%
Pyridine	18	60	78	23.1%	76.9%
Pyrimidine	12	24	36	33.3%	66.7%
Pyrrolidine	5	31	36	13.9%	86.1%
Tetrazole	1	9	10	10.0%	90.0%
Thiazole	5	39	44	11.4%	88.6%
Thiophene	3	17	20	15.0%	85.0%

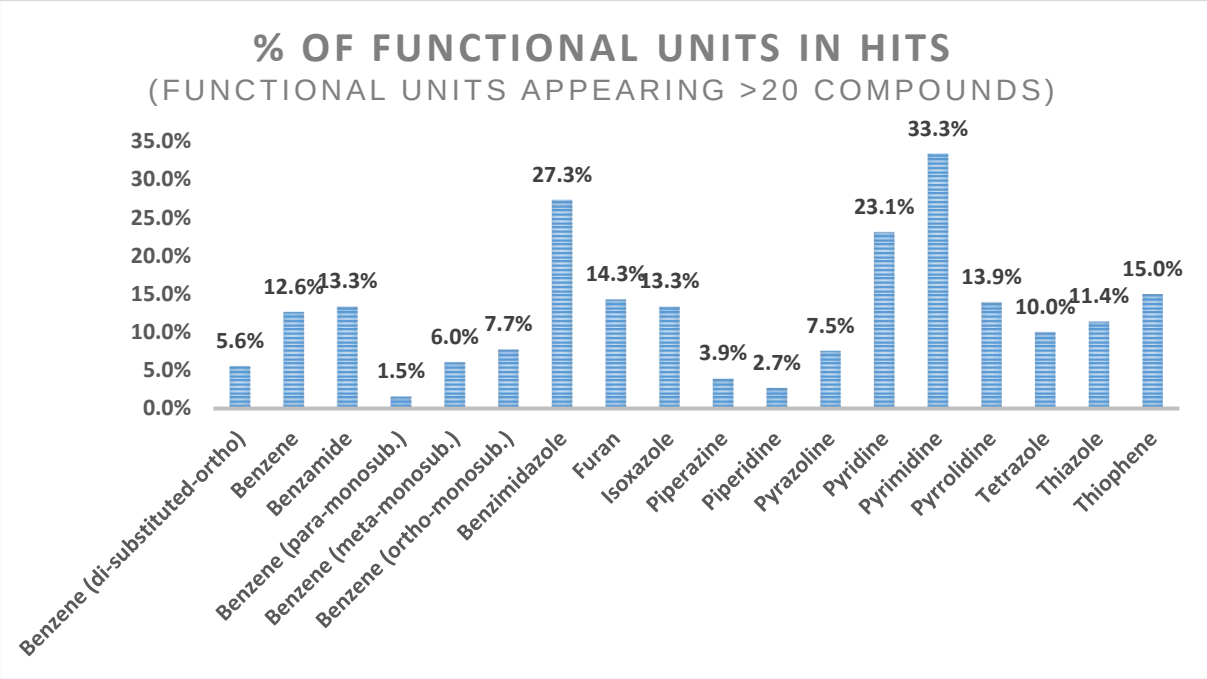

[1] A. Wacker, J. E. Weigand, S. R. Akabayov, N. Altincekic, J. K. Bains, E. Banijamali, O. Binas, J. Castillo-Martinez, E. Cetiner, B. Ceylan, L.-Y. Chiu, J. Davila-Calderon, K. Dhamotharan, E. Duchardt-Ferner, J. Ferner, L. Frydman, B. Fürtig, J. Gallego, J. T. Grün, C. Hacker, C. Haddad, M. Hähnke, M. Hengesbach, F. Hiller, K. F. Hohmann, D. Hymon, V. de Jesus, H. Jonker, H. Keller, B. Knezic, T. Landgraf, F. Löhr, L. Luo, K. R. Mertinkus, C. Muhs, M. Novakovic, A. Oxenfarth, M. Palomino-Schätzlein, K. Petzold, S. A. Peter, D. J. Pyper, N. S. Qureshi, M. Riad, C. Richter, K. Saxena, T. Schamber, T. Scherf, J. Schlagnitweit, A. Schlundt, R. Schnieders, H. Schwalbe, A. Simba-Lahuasi, S. Sreeramulu, E. Stirnal, A. Sudakov, J.-N. Tants, B. S. Tolbert, J. Vögele, L. Weiß, J. Wirmer-Bartoschek, M. A. Wirtz Martin, J. Wöhnert, H. Zetzsche, *Nucleic Acids Res.* **2020**, DOI 10.1093/nar/gkaa1013.

[2] O. B. Cox, T. Krojer, P. Collins, O. Monteiro, R. Talon, A. Bradley, O. Fedorov, J. Amin, B. D. Marsden, J. Spencer, F. Von Delft, P. E. Brennan, *Chem. Sci.* **2016**, *7*, 2322–2330.

[3] A.-S. Bretonnet, A. Jochum, O. Walker, I. Krimm, P. Goekjian, O. Marcillat, J.-M. Lancelin, *J. Med. Chem.* **2007**, *50*, 1865–1875.

[4] O. Binas, V. Jesus, T. Landgraf, A. E. Völklein, J. Martins, D. Hymon, J. Kaur Bains, H. Berg, T. Biedenbänder, B. Fürtig, S. Lakshmi Gande, A. Niesteruk, A. Oxenfarth, N. Shahin Qureshi, T. Schamber, R. Schnieders, A. Tröster, A. Wacker, J. Wirmer-Bartoschek, M. A. Wirtz Martin, E. Stirnal, K. Azzaoui, C. Richter, S. Sreeramulu, M. J. José Blommers, H. Schwalbe, *ChemBioChem* **2020**, cbic.202000476.

[5] T. Weinrich, E. A. Jaumann, U. Scheffer, T. F. Prisner, M. W. Göbel, *Chem. – A Eur. J.* **2018**, *24*, 6202–6207.

[6] D. R. Bullard, R. P. Bowater, *Biochem. J.* **2006**, *398*, 135–144.

[7] C. K. Ho, S. Shuman, *Proc. Natl. Acad. Sci.* **2002**, *99*, 12709 LP – 12714.

[8] E. E. Regulski, R. R. Breaker, *Methods Mol. Biol.* **2008**, *419*, 53–67.

[9] F. Wu, S. Zhao, B. Yu, Y. M. Chen, W. Wang, Z. G. Song, Y. Hu, Z. W. Tao, J. H. Tian, Y. Y. Pei, M. L. Yuan, Y. L. Zhang, F. H. Dai, Y. Liu, Q. M. Wang, J. J. Zheng, L. Xu, E. C. Holmes, Y. Z. Zhang, *Nature* **2020**, *579*, 265–269.

[10] R. Rangan, I. N. Zheludev, R. Das, *RNA* **2020**, *26*, 937–959.

[11] J. Hadfield, C. Megill, S. M. Bell, J. Huddleston, B. Potter, C. Callender, P. Sagulenko, T. Bedford, R. A. Neher, *Bioinformatics* **2018**, *34*, 4121–4123.

[12] T. L. Hwang, A. J. Shaka, *J. Magn. Reson. Ser. A* **1995**, *112*, 275–279.

[13] B. D. Nguyen, X. Meng, K. J. Donovan, A. J. Shaka, *J. Magn. Reson.* **2007**, *184*, 263–274.

[14] C. Dalvit, G. Fogliatto, A. Stewart, M. Veronesi, B. Stockman, *J. Biomol. NMR* **2001**, *21*, 349–359.

[15] C. Dalvit, *J. Biomol. NMR* **1998**, *11*, 437–444.

[16] T. D. Schneider, G. D. Stormo, L. Gold, A. Ehrenfeucht, *J. Mol. Biol.* **1986**, *188*, 415–431.